Supplemental Information File

Synthesis-Enabled Exploration of Chiral and Polar Multivalent Quaternary Sulfides

Georgiy Akopov[1,2], Nethmi W. Hewage[2], Philip Yox[1,2], Gayatri Viswanathan[1,2], Shannon J. Lee[1,2], Liam P. Hulsebosch[1,3], Sarah D. Cady[2], Alexander L. Paterson[1], Frédéric A. Perras[1], Wenqian Xu[4], Kui Wu[5], Yaroslav Mudryk[1], Kirill Kovnir[1,2,*]

[1]*Ames Laboratory, U.S. Department of Energy, Ames, IA 50011, United States.*

[2]*Department of Chemistry, Iowa State University, Ames, IA 50011, United States.*

[3]*Department of Physics, The State University of New York College at Buffalo, Buffalo, NY 14222.*

[4]*X-ray Science Division, Advanced Photon Source, Argonne National Laboratory, IL 60439, United States*

[5]*Hebei University, Baoding City, Hebei Province, 830011, China.*

*Corresponding authors: kovnir@iastate.edu

Table of Contents

Experimental Details

Tables

Figures

S1. Experimental Details

S1.1. Synthesis

The powders of $(RE)_6(TM)_x(Tt)Q_{14}$ (*RE* = Sc, Y and La; *TM* = all transition metals except for Y, Tc, and Os; *Tt* = Si, Ge and Sn; *Q* = S and Te) were synthesized using pre-arc-melted precursors and sulfur without flux, while crystals were grown using a salt flux synthesis from a pre-arc-melted precursor and sulfur.

Materials used: Tin powder (99.8%, Strem, USA), Sulfur powder (99.5%, Alfa Aesar, USA), Tellurium powder (99.5%, Matheson, Coleman & Bell, USA), Lanthanum Sulfide (99.9%, Strem, USA), Silicon powder (99.99%, Strem, USA), Titanium powder (99.9%, Strem, USA). Scandium, yttrium, and lanthanum pieces as well as all transition metals, silicon and germanium were acquired from the Materials Preparation Center at Ames Laboratory, which is supported by the US DOE Basic Energy Sciences: Scandium chunk (99.99%), Yttrium chunk (99.9999%), Lanthanum chunk (99.9999%), Titanium pellets (99.999%), Vanadium dish (99.95%), Chromium flakes (99.99%), Manganese pieces (99.99+%), Iron lumps (99.95%), Cobalt buttons (99.9%), Nickel pellets (99.99%), Copper pellets (99.995%), Niobium chunks (99.9%), Molybdenum rod (99.95%), Ruthenium powder (99.99%), Rhodium powder (99.99%), Palladium pieces (99.99%), Silver shot (99.99%), Hafnium plate (99.95%), Tantalum sheet (99.995%), Tungsten wire (99.95%), Rhenium pieces (99.9%), Iridium pieces (99.99%), Platinum shot (99.99%), Gold shot (99.99%), Silicon lumps (99.9999996%), and Germanium lumps (99.999%).

S1.1.1. Metal Silicide Precursors

RE-TM-Tt precursors were prepared using pieces of appropriate metals and tetrel. Samples with a total mass of 0.6 - 1 g were weighed out in a ratio of *RE* : *TM* : *Tt* = 6 : 1 : 2.05 (*RE* = Sc, Y and

La; *Tt* = Si, Ge and Sn; for all *TM*). Additionally, $(TM)_xSi_y$ (*TM* = Sc, Ti, V, Cr, Mn, Zr, Nb, Mo, Ru, Pd, La, Hf, Ta, and Re) precursors were prepared. **Table S1** lists the phase composition for most precursors used. Slight excess of tetrel was used to account for its evaporation during arc melting. The samples were then placed in an arc-melter on a copper hearth along with oxygen getter materials (zirconium metal). The arc-melter chamber was later sealed and evacuated for 20 minutes followed by purging with argon; this process was repeated 3 times to ensure no oxygen was present in the chamber. During arc-melting, the getters were melted first to ensure the absorbance of any trace oxygen, and then the samples were heated for $T \sim 1$ minute at a current of $I \sim 80$ Amperes (A) until molten, allowed to solidify, flipped and re-arced 2 more times to ensure homogeneity under a current of $I \sim 100$ A. The precursor ingots were then crushed into a powder using a steel Plattner-style diamond crusher.

Stability: The precursors were kept in desiccators outside of a glovebox. Most La-*TM*-Si precursors are stable with about a year shelf life. Samples more than a year old have been found to contain small amounts of lanthanum hydroxide. The notable exceptions are compositions with *TM* = Fe and Mn as well as Ge analogous, where most of the La is converted into the hydroxide at approximately 3 months mark.

S.1.1.2. Single Crystals

Single crystals of most compositions were grown using pre-arc-melted precursor, sulfur powder, and potassium iodide (KI) salt flux. The ratio of (precursor + sulfur) to KI flux was kept at 1 to 30 ratio by mass (for 0.1g of reactants 3g of KI was used). The reactants and KI salt were added to a silica ampule, which was sealed under vacuum. The samples were heated to 950 – 1050°C (depending on the transition metal used) over 12 hours, allowed to dwell over 72 - 120 hours and then cooled down to room temperature over 8 hours. The KI flux was washed with deionized water,

the sample was then vacuum filtered and allowed to dry. In most cases the crystals resemble rods with a hexagonal cross section, either narrow and long (1-3 mm) or short and bulky (1-2 mm). The crystals are typically dark colored, almost black, with a slight hint of color. The crystals with Cu, Ag, and Au have a transparent yellow-gold appearance. Some compositions, which produced clean bulk powder failed in crystal growth with KI: $La_6(TM)_xSi_2S_{14}$ (*TM* = Ru, Pd, and Ir).

S.1.1.3. Bulk Powders

Bulk powders of the materials were synthesized using pre-arc melted precursor and sulfur powder. Samples were prepared by loading the metal silicide precursor and sulfur in a fused silica ampoule in a 1 : 14 precursor to sulfur ratio. The ampoules were then flame sealed under vacuum. The samples were heated over 12 hours to 950 – 1050^{o}C (depending on the transition metal used), dwelled for 72 - 120 hours and then allowing them to cool to room temperature over 8 hours.

S.1.1.4. Control Test Reactions from Elements and Binary Precursors

Binary sulfides of Ti, Rh, and Si were prepared by combining powders of corresponding metal with S in 1 : 2.1 ratio. The ampoules were then flame sealed under vacuum. The samples were heated over 12 hours to 700 ^{o}C and dwelled for 72 hours and then allowing them to cool to room temperature over 8 hours. The products of the reactions were (TiS_2 + $Ti_8S_{3(impurity)}$) and (Rh_2S_3 + $RhS_{2(min)}$). The synthesis of SiS_2 was unsuccessful.

The synthesis of quaternary phases was performed from elements using the following ratio of reactants: 6La : 0.67(*TM*) : 2Si : 14S (*TM* = Ti and Rh). Furthermore, the synthetic attempt was performed using binary sulfides in the following ratio: $3La_2S_3$: $0.67TiS_2$: 2Si : 4S and $3La_2S_3$: $0.33Rh_2S_3$: 2Si : 4S. Elemental Si and S were used in lieu of SiS_2. The ampoules were then flame

sealed under vacuum. The samples were heated over 12 hours to 1050 ^{o}C and dwelled for 72 hours and then allowing them to cool to room temperature over 8 hours (**Figure S3F**).

S1.2. X-ray Diffraction

Powder X-ray diffraction (PXRD) was performed using a Rigaku Miniflex 600 with Cu-K_α radiation and a Ni-K_β filter. Sample holders were composed of zero-background silicon plates.

Single crystal X-ray diffraction (SCXRD) was performed using a Bruker D8 Venture diffractometer using Mo-K_α radiation. All crystal datasets were collected at 100 K under a N_2 stream. All datasets had ω-scans recorded at a 0.3 - 0.6 ° step width and were integrated with the Bruker SAINT software package.

Structure determination and refinement of the crystal structures were carried out using the SHELX suite of programs.[1] The site occupancy of transition metal was refined in all cases. For mono- and divalent metals occupancy of the two-fold site was found to be close to 100% and 50%, correspondingly, within few e.s.d. For trivalent metals, such as Sc, Ti, V, Cr, and Rh the refined occupancy was close to 33% (except for V). In addition, S3 atoms coordinating *TM* were found to have extremely elongated atomic displacement parameters (ADPs). This sulfur atom was further refined isotropically revealing a significant difference electron density peak indicating a split S site. Further refinement was performed with the constrains of 100% total occupancy and equivalent ADPs for split S3/S33 site which reduces the *R*-values and difference electron density peaks substantially. Occupancy of the split sites were found to be close to 67%/33% demonstrating good correlation with transition metal occupancy. In some cases, S33 site occupancy was restrained to be identical to the transition metal site occupancy. For *TM* = Sc, additional splitting of La site with 67/33% occupancy was necessary to properly describe electron density in the vicinity of La atomic

site. La site ADPs for other 3+ and 4+ metals were elongated in ab plane, but Sc case was the extreme. Final refinement was performed anisotropically for all atoms including transition metal and split S3/S33 site. Similar refinement logic was used for 4+ metal (Pt, Zr, Hf) which occupancy was close to 25%. Further details are provided in Table S1 and corresponding CIFs.

S1.3. Synchrotron Experiments at Advanced Photon Source at Argonne National Laboratory (APS ANL)

In-situ variable temperature PXRD experiments were carried out at the 17-BM beamline at APS ANL, λ = 0.24155 Å. To study the mechanism of formation of $La_6Rh_{0.7}Si_2S_{14}$, a small amount of precursor (with a nominal composition of $La_6Rh_{0.7}Si_2$) was ground in an agate mortar with S in 1 : 14 ratio, loaded in a 0.5mm (ID) capillary, and sealed under vacuum using a flame. For synthesis experiments, the following profile was used: heating at 10 ºC/min to 1000ºC, hold 10 minutes, then cooling at 100 ºC/min to room temperature.

S1.4.1. ^{29}Si and ^{45}Sc Solid State NMR

All solid-state nuclear magnetic resonance (NMR) spectroscopy experiments were carried out using a Bruker AVANCE III 400 MHz spectrometer using a 3.2 mm low-temperature magic angle spinning (MAS) probe operated at a temperature of approximately 100 K. ^{29}Si MAS NMR spectra were acquired with the use of a rotor-synchronized Hahn echo pulse sequence with a radiofrequency (rf) power of 50 kHz, a relaxation delay of 130 s, and an MAS frequency of 8 kHz. ^{45}Sc NMR experiments utilized a Bloch decay sequence, with a 10 μs central transition-selective excitation pulse, a 300 s relaxation delay, and an MAS rate of 14 kHz.

^{45}Sc NMR data were processed using the two-dimensional one-pulse (TOP) approach, as implemented in dmfit[2,3]. This enables for the separation of centerband signals belonging to the

central transition (CT) and satellite transitions (ST). The observed chemical shift of a given resonance from a specific transition of a quadrupolar nucleus is given by

$$\delta_{\mathrm{obs}} = \delta_{\mathrm{iso}} - \frac{3P_{\mathrm{Q}}^2}{40\nu_0^2}\frac{I(I+1) - 9m(m-1) - 3}{I^2(2I-1)^2}10^6\mathrm{ppm/Hz}$$

where I = 7/2 for ^{45}Sc and m = 1/2 for the central transition (CT) and 3/2 (or -1/2) for the inner satellite transitions (ST). As such we have the following peak positions for the CT and inner ST:

$$\delta_{\mathrm{obs,CT}} = \delta_{\mathrm{iso}} - \frac{P_{\mathrm{Q}}^2}{\nu_0^2}\frac{10^6\mathrm{ppm/Hz}}{392}$$

$$\delta_{\mathrm{obs,ST}} = \delta_{\mathrm{iso}} - \frac{P_{\mathrm{Q}}^2}{\nu_0^2}\frac{10^6\mathrm{ppm/Hz}}{980},$$

and their difference is given by

$$\delta_{\mathrm{obs,ST}} - \delta_{\mathrm{obs,CT}} = \frac{3P_{\mathrm{Q}}^2}{\nu_0^2}\frac{10^6\mathrm{ppm/Hz}}{1960}.$$

Having extracted the inner ST and CT centerbands through TOP, the quadrupolar product (P_{Q}) is readily determined, along with the isotropic chemical shift δ_{iso}. P_{Q} is related to the quadrupolar coupling constant (C_{Q}) as $P_{\mathrm{Q}} = C_{\mathrm{Q}}\sqrt{1+\frac{\eta^2}{3}}$ and ranges from C_{Q} to 1.15C_{Q}; η is the quadrupolar asymmetry parameter.

S1.4.2. Density Functional Theory

Density-functional theory (DFT) calculations were carried out using the CASTEP software package[4]. Simulations of NMR parameters were performed using the gauge-including projector-augmented wave (GIPAW) approach[5], as implemented in CASTEP[6]. The default on-the-fly-

generated ultrasoft pseudopotentials were used for all atoms, and the Perdew-Burke-Ernzerhof (PBE)[7] generalized gradient approximation exchange-correlation functional was used for all calculations. Prior to performing magnetic shielding and electric field gradient calculation, the fractional coordinates of the atoms were optimized using a plane-wave kinetic energy cut-off of between 360 eV and 570 eV, depending on the identity of the transition metal, and a 2×2×2 Γ-centered *k*-point mesh. The atomic positions were optimized using a total energy convergence tolerance of 5×10^{-6} eV/atom, a maximum ionic force tolerance of 0.01 eV/Å, and a maximum atomic displacement tolerance of 5×10^{-4} Å. Subsequent NMR parameter calculations used a similar plane-wave energy cut-off, but a much denser *k*-point grid, with a *k*-point spacing of 0.03 $Å^{-1}$.

^{29}Si magnetic shielding constants (σ_{iso}) were converted to chemical shifts (δ_{iso}) through the usual relation: $\delta_{iso} = \sigma_{ref} - \sigma_{iso}$, where σ_{ref} is the shielding of a reference compound with a known chemical shift. In this study the shielding of SiS_2 (σ_{ref} = 315.87 ppm, δ_{iso} = -21.1 ppm[8]) was used as a secondary reference (relative to tetramethylsilane), based on the structure reported by Evers *et al*.[9] ^{45}Sc shielding was not studied computationally due to the difficulty in finding a suitable reference material.

^{45}Sc EFGs were calculated by generating several 2×2×2 supercells with varying occupancy of the Sc *TM* site. The C_Q and η for each individual Sc site were calculated for each structure. The average values are reported in **Table S6**.

S.1.5. Scanning Electron Microscopy/Energy Dispersive Spectroscopy (SEM/EDS)

Elemental analysis of samples was conducted using a FEI Quanta 250 field emission-SEM with EDS detector (Oxford X-Max 80, ThermoFischer Scientific, Inc., USA) and analyzed using the

Aztec software. Powder samples were mounted in epoxy, polished to a level surface, and coated with a conductive layer of carbon. Large crystals were mounted on double-sided carbon tape. An accelerating voltage of 15kV was used to study all samples.

S1.6. Solid-State Diffuse Reflectance Spectroscopy

The UV/Vis diffuse reflectance spectra were measured from 200-1080 nm with a BLACK-Comet C-SR-100 spectrometer. Powder samples were finely ground and flattened on a microscope slide. Band gaps were estimated through extrapolation of the linear slope in the corresponding Tauc plots by plotting $(A\textit{hv})^{1/r}$ vs $\textit{hv}$ where r = ½ for direct and r = 2 for indirect band gaps.

S1.7. SQUID Magnetometry

Magnetic properties were obtained using SQUID magnetometer, model MPMS XL-7, manufactured by Quantum Design. The powder samples were placed into quartz sample holders and sealed with Teflon tape. Magnetization was measured as a function of temperature in applied magnetic field of H = 1 kOe and 20 kOe from 2 to 300 K (on heating) and, isothermally, as a function of applied magnetic field at 2 and 300 K between -70 and 70 kOe (full hysteresis loop). AC susceptibility was measured between 2 and 50 K wit H_{ac} = 5 Oe, H_{dc} = 0, and f = 100 Hz.

S1.8. EPR Analysis

Electron paramagnetic resonance (EPR) spectra were collected using an X-band ELEXYS E580 EPR Spectrometer (Bruker BioSpin) equipped with an SHQE resonator operating at 9.4 GHz, and a Bruker variable temperature accessory for heating/cooling. Powder samples were loaded into a 4 mm suprasil synthetic quartz tube (SP Wilmad-LabGlass) to minimize background signal from naturally occurring metals. Spectra were acquired with a sweep width of 4000 G, center field of 3350 G, receiver gain of 40 dB, 4096 points, sweep time of 83.9 s, time constant of 0.04 ms, and

5 G modulation amplitude. The 298 K spectrum was acquired with 1.986 mW microwave power and 1 scan, while the 110 K spectrum was acquired with 4.975 mW microwave power and 4 scans.

S1.9 Second Harmonic Generation (SHG) and Laser Damage Threshold (LDT)

Through the Kurtz and Perry method, powder SHG responses were investigated by a Q-switch laser (2.09 μm, 3 Hz, 50 ns) with different particle sizes, including 38−55, 55−88, 88−105, 105−150, 150−200, and 200−250 μm. The $AgGaS_2$ crystal was ground and sieved into the same size range as the reference. The LDTs were evaluated on powder sample (150−200 μm) with a pulsed YAG laser. Similar size of $AgGaS_2$ was chosen as the reference. To adjust different laser beams, an optical concave lens is added into the laser path. The damage spot is measured by the scale of optical microscope.

Table S1A. SCXRD data collection and refinement parameters for $La_6(TM)_xSi_2S_{14}$ (*TM* = Sc, Ti, V, Cr, Mn, Fe, Co, and Ni; x = 2 – 0.5)

	$La_6Sc_{0.65(1)}Si_2S_{14}$	$La_6Ti_{0.62(1)}Si_2S_{14}$	$La_6V_{0.77(1)}Si_2S_{14}$	$La_6Cr_{0.66(1)}Si_2S_{14}$	$La_6Mn_{0.98(1)}Si_2S_{14}$	$La_6Fe_{1.05(1)}Si_2S_{14}$	$La_6Co_{1.01(1)}Si_2S_{14}$	$La_6Ni_{0.99(1)}Si_2S_{14}$
CSD-number	2089790	2089782	2089797	2089783	2089795	2089796	2089784	2089793
Space group	$P6_3$							
λ (Å)	Mo-Kα: 0.71073							
***T* (K)**	100(2)							
***a* (Å)**	10.3383(5)	10.2970(5)	10.2960(4)	10.2888(12)	10.3337(4)	10.2991(3)	10.3141(11)	10.2725(6)
***c* (Å)**	5.7459(4)	5.7720(3)	5.7356(3)	5.7503(9)	5.7285(3)	5.7389(3)	5.7313(10)	5.7287(4)
***V* (Å^{-3})**	531.85(6)	529.9(5)	526.56(5)	527.17(15)	529.76(5)	527.18(4)	528.02(15)	523.53(7)
Z	1							
ρ (g•cm^{-3})	4.269	4.287	4.345	4.324	4.364	4.401	4.395	4.432
Absorption correction	multi-scan							
μ (mm^{-1})	13.437	13.515	13.704	13.690	13.860	14.062	14.105	14.333
θ (°)	2.27 – 40.13	2.29 – 32.99	2.28 – 40.24	2.29 – 33.05	2.28 – 40.36	2.28 – 40.23	2.18 – 33.07	2.29 – 32.95
Data / param.	1805/46	1339/43	1789/40	1340/42	1795/38	1787/38	1337/38	1340/38
***R*$_1$**	0.019	0.015	0.020	0.021	0.026	0.019	0.011	0.037
***wR*$_2$**	0.031	0.028	0.036	0.034	0.044	0.036	0.025	0.047
Goodness-of-fit	1.05	1.05	1.05	1.05	1.03	1.12	1.13	1.05
Flack Param.	0.01(1)	0.03(2)	-0.006(11)	-0.01(1)	0.02(3)	0.01(2)	0.010(8)	0.01(3)
Diff. peak/hole (e•Å^{-3})	1.09/-1.21	0.93/-1.29	2.02/-1.83	1.76/-2.07	1.25/-1.78	0.83/-1.52	0.71/-0.60	1.67/-1.51

Table S1B. SCXRD data collection and refinement parameters for $La_6(TM)_x(Tt)_2S_{14}$ (*TM* = Zr, Rh, Pd, Hf, Pt, Cu, Ag, and Au; *Tt* = Si, Ge, and Sn; x = 2 – 0.5)

	$La_6Zr_{0.52(1)}Si_2S_{14}$	**$La_6Rh_{0.69(1)}Si_2S_{14}$**	**$La_6Hf_{0.48(2)}Si_2S_{14}$**	**$La_6Pt_{0.53(1)}Si_2S_{14}$**	**$La_6Cu_{1.97(1)}Si_2S_{14}$**	**$La_6Au_{1.92(3)}Si_2S_{14}$**	**$La_6Au_{1.98(2)}Ge_2S_{14}$**	**$La_6Au_{1.94(2)}Sn_2S_{14}$**
CSD-number	2089794	2089787	2089792	2089791	2089788	2089789	2089786	2089785
Space group	$P6_3$							
λ (Å)	Mo-Kα: 0.71073							
***T* (K)**	100(2)							
***a* (Å)**	10.3189(6)	10.2507(5)	10.3188(6)	10.2530(3)	10.3231(14)	10.3804(15)	10.3905(16)	10.4001(19)
***c* (Å)**	5.7543(4)	5.7490(3)	5.7612(5)	5.7717(3)	5.7991(8)	5.8250(14)	5.8848(10)	6.0178(14)
***V* (Å^{-3})**	530.63(7)	523.15(16)	531.25(8)	525.46(4)	535.19(16)	543.6(2)	550.22(19)	563.7(2)
Z	1							
ρ (g•cm^{-3})	4.337	4.474	4.451	4.557	4.541	5.238	5.479	5.597
Absorption correction	multi-scan							
μ (mm^{-1})	13.522	13.996	15.644	16.921	15.074	25.789	28.446	27.056
θ (°)	2.28 – 32.78	2.29 – 33.11	2.28 – 32.49	2.29 – 33.05	2.28 – 33.18	2.27 – 33.18	2.27 – 33.24	2.27 – 33.25
Data / param.	1189/42	1340/43	1289/41	1220/42	1362/39	1372/39	1364/39	1436/39
R_1	0.024	0.018	0.026	0.039	0.012	0.013	0.013	0.016
wR_2	0.036	0.029	0.043	0.086	0.023	0.025	0.024	0.025
Goodness-of-fit	1.05	1.07	1.07	1.11	1.11	0.97	1.09	1.02
Flack Param.	0.03(3)	0.02(3)	0.04(4)	0.04(5)	0.026(15)	0.012(6)	0.019(6)	0.020(6)
Diff. peak/hole (e•Å^{-3})	0.97/1.10	1.51/-1.96	1.05/-1.49	2.56/-2.04	0.62/-0.49	1.81/-0.74	0.95/-0.76	2.12/-0.96

Table S2. Phase composition of precursors used for the synthesis of quaternary phases.

RE	***TM***	**Nominal Composition**	**Crystalline Phases Identified by PXRD in Brittle Fraction of Precursor**
Sc	-	5Sc : 3Si	Sc_5Si_3
	Ti	6Sc : Ti : 2Si	Sc_5Si_3 + Sc
	Mn	6Sc : Mn : 2Si	Sc_5Si_3 + Sc + $ScMn_2$
	Fe	6Sc : Fe : 2Si	Sc_5Si_3 + $FeSi_2$ + Sc_5Fe
	Co	6Sc : Co : 2Si	Sc_5Si_3 +Sc_2Co + ScCo
	Ni	6Sc : Ni : 2Si	Sc_5Si_3 + $ScNiSi_3$
	Cu	6Sc : 2Cu : 2Si	Sc_5Si_3 + ScCu
	Rh	6Sc : Rh : 2Si	Sc_5Si_3 + $Sc55.8Rh_{13.8}$
	Ag	6Sc : 2Ag : 2Si	ScAg + Sc_5Si_3
	Ir	6Sc : Ir : 2Si	Sc_5Si_3 + Sc_3IrSi_3 + Ir_3Si_5
	Au	6Sc : 2Au : 2Si	ScAu + Sc_5Si_3
Y	Cr	6Y : Cr : 2Si	Y_5Si_3 + Y + Cr + Si
	Mn	6Y : Mn : 2Si	Y_5Si_3 + Y + Si + YSi_2
	Fe	6Y : Fe : 2Si	Y_5Si_3 + YFe_2 + Y
	Co	6Y : Co : 2Si	Y_5Si_3 + Y_3Co
	Ni	6Y : Ni : 2Si	Y_5Si_3 + Y_3Ni + Si + Y
	Cu	6Y : 2Cu : 2Si	Y_5Si_3 + YCu + YSi_2
La	-	5La : 3Si	La_5Si_3 + La_5Si_4
	Sc	6La : Sc : 2Si	La_5Si_3 + Sc_5Si_3 + LaScSi
		6La : Sc : 2Ge	La_5Ge_3 + LaScGe + Ge
	Ti	6La : Ti : 2Si	La_5Si_3 + La + Ti
		Ti : 2Si	$TiSi_2$ + TiSi
	V	6La : V : 2Si	La_5Si_3 + Si
		5V : 3Si	V_5Si_3 + Si
	Cr	6La : Cr : 2Si	La_5Si_3 + Cr
		Cr : Si	CrSi + Cr_5Si_3
	Mn	6La : Mn : 2Si	La_5Si_3 + La + Mn
		La : Mn : 2Si	$LaMn_2Si_2$ + LaSi + $LaSi_2$
		Mn : Si	$MnSi_{1.733}$ + MnSi + Si
		6La : Mn : 2Ge	La_3Ge + La_5Ge_3 + $Mn_{11}Ge_8$
		6La : Mn : 2Sn	La_5Sn_3 + Mn_3Sn_2
	Fe	6La : Fe : 2Si	La_5Si_3 + La + $LaFe10.6Si_{2.4}$
		6La : Fe : 2Ge	La_3Ge + $La_{15}FeGe_9$
		6La : Fe : 2Sn	La_5Sn_3 + FeSn + Fe + La
	Co	6La : Co : 2Si	$La_5Co_{0.3}Si_{2.7}$ + La_3Co
		6La : Co : 2Ge	La_5Ge_3 + Ge + La_3Co
		6La : Co : 2Sn	La_3Co + La_5Sn_3 + La + La_3Sn_5
	Ni	6La : Ni : 2Si	$La_5Ni_{0.26}Si_{2.735}$ + La_3Ni
		6La : Ni : 2Ge	Ge + La_3Ni + La_5Ge
		6La : Ni : 2Sn	La_5Sn_3 + La_7Ni_3
	Cu	6La : 2Cu : 2Si	La_5Si_3 + $LaCu_4$
		6La : 2Cu : 2Ge	Ge + La_5Ge_3 + La(CuGe)

		6La : 2Cu : 2Sn	La_5Sn_3 + LaCu + Cu_6Sn_5
	Zr	6La : Zr : 2Si	La_5Si_3 + Zr_5Si_3
		Zr : Si	ZrSi + Zr_5Si_3
	Nb	6La : Nb : 2Si	La_5Si_3 + Nb_5Si_3
		Nb : Si	Nb_5Si_3 + $NbSi_2$
	Mo	6La : Mo : 2Si	La_5Si_3 + Si
		Mo : 2Si	$MoSi_2$ + Mo + Si
	Ru	6La : Ru : 2Si	Ru + La_5Si_3 + Si
		Ru : Si	RuSi + Ru_2Si_3 + Ru_5Si_3
		6La : Ru : 2Ge	Ru + LaGe + La_3Ge
	Ru	6La : Ru : 2Sn	La_5Sn_3 + Sn + La + $LaRuSn_3$ + $La_3Ru_4Sn_{13}$
	Rh	6La : Rh : 2Si	La_5Si_3 + La_7Rh_3
La		6La : Rh : 2Ge	La_3Ge + La_3Rh + Ge
		6La : Rh : 2Sn	La_5Sn_3 + Sn + La_7Rh_3 + $La_{16}Rh_8Sn_3$
	Pd	6La : Pd : 2Si	Si + La + $LaSi_2$ + La_7Pd_3
		2Pd : Si	Pd_2Si
		6La : Pd : 2Ge	La_5Ge_3 + La_7Pd_3
		6La : Pd : 2Sn	La_5Sn_3 + La_7Pd_3 + La_3Sn_4
	Ag	6La : 2Ag : 2Si	LaAg + $LaSi_2$ + Si + La
		6La : 2Ag : 2Ge	La_4Ge_3 + LaAg + LaGe + Ge
		6La : 2Ag : 2Sn	La_5Sn_3 + LaAg
	Hf	6La : Hf : 2Si	La_5Si_3 + Hf_5Si_3
		Hf : Si	HfSi + Hf_5Si_4 + $HfSi_2$
	Ta	6La : Ta : 2Si	La_5Si_3 + Ta_5Si_3
		Ta : Si	Ta_5Si_3 + $TaSi_2$ + Ta_2Si
	W	6La : W : 2Si	La_5Si_3
		W : 2Si	WSi_2 + W_5Si_3 + Si
	Re	6La : Re : 2Si	La_5Si_3 + La + Re
		4Re : 7Si	$ReSi_2$ + ReSi + Si + Re
		6La : Re : 2Ge	La_3Ge + La_5Ge_3 + $ReGe_2$
		6La : Re : 2Sn	La_5Sn_3
	Ir	6La : Ir : 2Si	La_5Si_3 + La + Si + Ir_2Si
		6La : Ir : 2Ge	La_5Ge_3 + La + Ge + La_3Ir_2 + La_2Ir_7 + La_5Ir_2
		6La : Ir : 2Sn	$IrSn_2$ + La_5Sn_3 + La_3Sn + Sn
	Pt	6La : Pt : 2Si	La_5Si_3 + La_7Pt_3
		6La : Pt : 2Ge	La + La_5Ge_4 + Ge + Pt_3Ge
		6La : Pt : 2Sn	La_5Sn_3 + La_7Pt_3 + $La_{11}Sn_{10}$
	Au	6La : 2Au : 2Si	La_3Si_2 + $LaSi_2$ + $Au_{51}La_{14}$ + Si
		6La : 2Au : 2Ge	Ge + La_5Ge_4 + LaAuGe + $AuLa_2$
		6La : 2Au : 2Sn	La_3Sn + Sn + La_5Sn_3 + $AuSn_2$

Table S3A. Synthesis conditions for phase formation of $La_6(TM)_x(Tt)_2S_{14}$ (*TM* = Group 3 – 11, *Tt* = Si, Ge and Sn; x = 2 – 0.5). Quaternary phases are highlighted in bold for cases where they are the major products.

TM	*Tt*	Precursor	Max. Temp. (ºC)	Dwell Time (hrs)	Phases in Product
Sc	Si	$La_6Sc_{0.7}Si_2$	1000	72	**$La_6Sc_{0.67}Si_2S_{14}$** + S_8 + $LaScS_3$
	Ge	La_6ScGe_2 + KI	1000	72	**$La_6Sc_{0.67}Ge_2S_{14}$** + S_8 + La_2S_3 + $LaScS_3$
Ti	Si	$La_6Ti_{0.7}Si_2$	1050	72	**$La_6Ti_{0.67}Si_2S_{14}$**
V	Si	La_5Si_3 + V_5Si_3	1000	72	**$La_6V_{0.77}Si_2S_{14}$** + LaS_2 + S_8
Cr	Si	$La_6Cr_{0.7}Si_2$	1050	72	**$La_6CrSi_2S_{14}$** + S_8
Zr	Si	La_5Si_3 + ZrSi	1000	72	**$La_6Zr_{0.5}Si_2S_{14}$** + La_2SiS_5 + ZrS_2 + La_2ZrS_5
Nb	Si	La_5Si_3 + NbSi	1000	72	La_2SiS_5 + $La_8Nb_7S_{22}$ + S_8
Mo	Si	La_5Si_3 + $MoSi_2$	1000	72	La_2SiS_5 + S_8 + MoS_2
Hf	Si	La_5Si_3 + 0.5HfSi	1000	72	**$La_6Hf_{0.5}Si_2S_{14}$** + La_2SiS_5
Ta	Si	La_5Si_3 + TaSi	1000	72	La_2SiS_5 + $TaSi_2$
W	Si	La_5Si_3 + WSi_2	1000	72	La_2SiS_5 + WSi_2
Mn	Si	La_5Si_3 + MnSi	1000	72	**$La_6MnSi_2S_{14}$** + La_2SiS_5(min)
	Ge	La_6MnGe_2	1050	72	**$La_6MnGe_2S_{14}$** + La_2S_3 + MnS
	Sn	La_6MnSn_2	1050	72	**$La_6MnSn_2S_{14}$**
Fe	Si	La_6FeSi_2	1050	72	**$La_6FeSi_2S_{14}$** + LaS_2
	Ge	La_6FeGe_2	1000	72	**$La_6FeGe_2S_{14}$** + GeS_2 + S_8
	Sn	La_6FeSn_2	1000	72	**$La_6FeSn_2S_{14}$** + La_2S_3
Co	Si	La_6CoSi_2	1050	0	**$La_6CoSi_2S_{14}$** + LaS_2
	Ge	La_6CoGe_2	1000	72	**$La_6CoGe_2S_{14}$** + S_8
	Sn	La_6CoSn_2	1000	72	**$La_6CoSn_2S_{14}$** + La_4CoS_7 + SnS
Ni	Si	La_6NiSi_2	1050	72	**$La_6NiSi_2S_{14}$** + La_4NiS_7
	Ge	La_6NiGe_2	1000	72	**$La_6NiGe_2S_{14}$**
	Sn	La_6NiSn_2	1000	72	**$La_6NiSn_2S_{14}$** + La_2S_3
Ru	Si	La_6RuSi_2	1050	72	**$La_6RuSi_2S_{14}$** + S_8
	Ge	La_6RuGe_2	1050	72	La_2GeS_5 + La_2S_3 + S_8
	Sn	La_6RuSn_2	1100	72	La_3Sn_4 + La_2SnS_5 + RuS_2
Rh	Si	$La_6Rh_{0.7}Si_2$	1000	72	**$La_6Rh_xSi_2S_{14}$** + S_8
	Ge	La_6RhGe_2	1000	72	**$La_6Rh_xGe_2S_{14}$** + LaS + GeS_2
	Sn	La_6RhSn_2	1050	72	**$La_6Rh_xSn_2S_{14}$** + $La_{16}Rh8Sn_3$
Pd	Si[a]	La_6PdSi_2	1050	72	**$La_6PdSi_2S_{14}$** + La_4PdS_7 + Pd_3S_2
	Ge	La_6PdGe_2	1050	72	**$La_6PdGe_2S_{14}$** + $LaPd_3S_4$ +La_2S_3
	Sn	La_6PdSn_2	900	72	$LaPd_3S_4$ + La_2SnS_5 + LaS_2 + Sn
Re	Si	La_6ReSi_2	1000	72	La_2SiS_5 + ReS_2 + S_8
	Ge	La_6ReGe_2	1000	72	La_2GeS_5 + $La_4Ge_3S_{12}$ + LA_2S_3 + Ge
	Sn	La_6ReSn_2	1050	72	La_2S_3 + ReS_2 + Sn + S_8
Ir	Si	$La_6Ir_{0.7}Si_2$	1000	72	**$La_6Ir_{0.67}Si_2S_{14}$** + LaS_2 + S_8
	Ge	La_6IrGe_2	1000	72	**$La_6Ir_xGe_2S_{14}$** + La_2S_3 + Ge
	Sn	La_6IrSn_2	900	72	La_2Sn_5 + La_2S_3 + IrS + SnS
Pt	Si	La_6PtSi_2	1000	72	**$La_6Pt_{0.5}Si_2S_{14}$** + PtS + La_2S_3

	Ge	La_6PtGe_2	1000	72	**$La_6Pt_xGe_2S_{14}$** + PtGeS + La_2S_3
	Sn	La_6PtSn_2	1050	72	PtSnS + La_2S_3 + La_2SnS_5 + $LaSn_3$
Cu	Si	$La_6Cu_2Si_2$	1000	72	**$La_6Cu_2Si_2S_{14}$**
	Ge	$La_6Cu_2Ge_2$	1000	72	**$La_6Cu_2Ge_2S_{14}$** + S_8
	Sn	$La_6Cu_2Sn_2$	1000	72	**$La_6Cu_2Sn_2S_{14}$** + $CuSnS_{3.6}$
Ag	Si	$La_6Ag_2Si_2$	1000	72	**$La_6Ag_2Si_2S_{14}$**
	Ge	$La_6Ag_2Ge_2$	1000	72	**$La_6Ag_2Ge_2S_{14}$** + S_8
	Sn	$La_6Ag_2Sn_2$	1000	72	**$La_6Ag_2Sn_2S_{14}$** + SnS
Au	Si	$La_6Au_2Si_2$	1000	72	**$La_6Au_2Si_2S_{14}$** + LaS_2
	Ge	$La_6Au_2Ge_2$	1000	72	**$La_6Au_2Ge_2S_{14}$**
	Sn	$La_6Au_2Sn_2$	1000	72	**$La_6Au_2Sn_2S_{14}$** + SnS

Table S3B. Selected results for the attempts to form $Sc_6(TM)_xSi_2S_{14}$ (unsuccessful) and $Y_6(TM)_xSi_2S_{14}$ (successful) for *TM* = Ti, Cr – Ni, Rh, Ir, Cu, Ag, and Au. Quaternary phases are highlighted in bold for cases where they are the major products.

RE	***TM***	**Precursor**	**Max. Temp. (ºC)**	**Dwell Time (hrs)**	**Phases in Product**
Sc	Ti	Sc_6TiSi_2	900	72	Sc_2S_3
			1050	96	$ScS + Sc_2S_3 + TiS_{1.5} + S_8$
	Mn	Sc_6MnSi_2	750	72	$Sc_2S_3 + MnS + MnSc_2S_4$
			1000	72	$MnS + MnSc_2S_4 + Mn_2SiS_4 + SiS_2 + Sc_2S_3$
	Fe	Sc_6FeSi_2	750	72	$Sc_2S_3 + FeSc_2S_4 + Sc_5Si_3$
			1000	72	$FeScS_4 + Sc_2S_3$
	Co	Sc_6CoSi_2	750	72	$Sc_2S_3 + CoS_2$
			1000	72	$Sc_2S_3 + CoS_2 + SiS_2$
	Ni	Sc_6NiSi_2	750	72	$Sc_2S_3 + NiS_2$
			1000	72	$Sc_2S_3 + S_8 + NiSc + NiS_2$
	Rh	Sc_6RhSi_2	900	72	$Sc_2S_3 + Rh_2S_3 + RhS_2$
			1050	96	$Sc_2S_3 + Rh_2S_3 + ScS + S_8$
	Ir	Sc_6IrSi_2	900	72	$Sc_2S_3 + IrS_2 + SiS_2$
			1050	96	$ScS + IrS_2 + Sc_2S_3 + SiS_2$
	Cu	$Sc_6Cu_2Si_2$	900	72	$ScS + Sc_2S_3 + Si + Sc + Cu_5Si_3S_8$
			1050	96	$ScS + CuScS_2 + Sc + S_8 + Sc_2S_3 + SiO_2$
	Ag	$Sc_6Ag_2Si_2$	900	72	$ScS + Sc_2S_3 + Si$
			1050	96	$Sc_2S_3 + SiO_2 + SiS_2$
	Au	$Sc_6Au_2Si_2$	900	72	$Au + ScS + Sc_2S_3 + S_8$
			1050	96	$Au + ScS + Sc_2S_3$
Y	Cr	Y_6CrSi_2	1050	72	$\mathbf{Y_6Cr_{0.67}Si_2S_{14}} + Y_2S_3$
	Mn	Y_6MnSi_2	1050	72	$\mathbf{Y_6MnSi_2S_{14}} + Y_2S_3$
	Fe	Y_6FeSi_2	1050	72	$\mathbf{Y_6FeSi_2S_{14}} + Y_2S_3$
	Co	Y_6CoSi_2	1050	72	$\mathbf{Y_6CoSi_2S_{14}} + Y_2S_3$
	Ni	Y_6NiSi_2	1050	72	$\mathbf{Y_6NiSi_2S_{14}} + Y_2S_3$
	Cu	$Y_6Cu_2Si_2$	1050	72	$\mathbf{Y_6Cu_2Si_2S_{14}}$

Table S3C. Synthesis conditions for the attempts to form tellurides $La_6(TM)_xSi_2Te_{14}$.

TM	Precursor	Max. Temp. (°C)	Dwell Time (hrs)	Phases in Product
Co	La_6CoSi_2	750	72	$LaTe_2 + La_2Te_5 + LaTe_3 + CoTe_2$
		900	72	$(La_2Te_3)_{0.9} + LaTe_2 + Si + Co$
		1050	72	$LaTe_2 + LaTe_3 + CoSi_2$
Ni	La_6NiSi_2	750	72	$LaTe_3 + NiTe_2 + Te$
		900	72	$LaTe_3 + NiTe_2 + Si$
		1050	72	$LaTe_2 + LaTe_3 + LaNi_7Si_6 + La_6Ni_2Si_3 + LaTe$
Cu	$La_6Cu_2Si_2$	750	72	$LaTe_2 + Si_2Te_3 + Cu_2SiTe_3$
		900	72	$La_2Te_5 + Cu_2SiTe_3 + Cu + LaTe_3 + Cu_3Si$
		1050	72	$LaTe_2 + Cu_7Te_4$

Table S4. EDS composition summary for $La_6(TM)_x(Tt)_2S_{14}$ (*TM* = Group 3 – 11, *Tt* = Si, Ge and Sn). All compositions are normalized to 6 La atoms. Errors are given in parenthesis.

RE	*TM*	*Tt*	Average EDS Composition	*TM* content from SCXRD
La	Sc	Si	$La_6Sc_{0.65(1)}Si_{0.95(6)}S_{13.58(10)}$	0.67
La	Ti	Si	$La_6Ti_{0.64(5)}Si_{2.01(7)}S_{13.18(7)}$	0.67
La	V	Si	$La_6V_{0.69(4)}Si_{1.96(2)}S_{13.13(10)}$	0.77
La	Cr	Si	$La_6Cr_{0.64(3)}Si_{1.94(2)}S_{13.16(10)}$	0.67
La	Mn	Sn	$La_6Mn_{0.91(5)}Sn_{2.13(1)}S_{13.09(13)}$	1.0
La	Co	Si	$La_6Co_{0.92(2)}Si_{2.05(2)}S_{13.71(7)}$	1.0
La	Ni	Si	$La_6Ni_{0.93(3)}Si_{1.93(6)}S_{13.17(24)}$	1.0
La	Zr	Si	$La_6Zr_{0.48(2)}Si_{1.97(5)}S_{12.95(4)}$	0.5
La	Ru	Si	$La_6Ru_{0.86(6)}Si_{2.01(7)}S_{13.15(11)}$	N/A
La	Rh	Si	$La_6Rh_{0.67(2)}Si_{1.95(3)}S_{13.04(12)}$	0.67
La	Rh	Ge	$La_6Rh_{0.67(2)}Ge_{1.78(2)}S_{13.15(9)}$	0.67
La	Rh	Sn	$La_6Rh_{0.54(2)}Sn_{2.21(7)}S_{13.18(3)}$	N/A
La	Pd	Si	$La_6Pd_{0.99(4)}Si_{1.98(4)}S_{13.12(12)}$	1.0
La	Hf	Si	$La_6Hf_{0.47(3)}Si_{2.08(2)}S_{13.04(16)}$	0.5
La	Ir	Si	$La_6Ir_{0.69(2)}Si_{1.94(3)}S_{13.18(8)}$	0.67
La	Ir	Ge	$La_6Ir_{0.76(8)}Ge_{1.80(5)}S_{13.30(23)}$	N/A
La	Pt	Si	$La_6Pt_{0.58(1)}Si_{1.96(2)}S_{13.43(4)}$	0.5
La	Cu	Si	$La_6Cu_{1.81(15)}Si_{2.04(4)}S_{13.70(16)}$	2.0
La	Cu	Ge	$La_6Cu_{1.63(5)}Ge_{2.29(32)}S_{14.17(71)}$	2.0
La	Au	Si	$La_6Au_{1.98(2)}Si_{2.22(4)}S_{14.16(5)}$	2.0
La	Au	Ge	$La_6Au_{1.88(2)}Ge_{1.74(2)}S_{13.78(6)}$	2.0
La	Au	Sn	$La_6Au_{1.76(6)}Sn_{2.04(4)}S_{13.40(13)}$	2.0

Table S5. Experimental and DFT-calculated ^{29}Si chemical shifts.

Sample	Experimental	Calculated	
	δ_{iso}(^{29}Si) / ppm	δ_{iso}(^{29}Si) / ppm	σ_{iso}(^{29}Si) / ppm
$La_6Cu_2Si_2S_7$	3.0	2.6	313.3
$La_6Ag_2Si_2S_7$	4.9	9.8	306.1
$La_6Au_2Si_2S_7$	7.7	12.5	303.5
$La_6RhSi_2S_{14}$ [a]	0.4		
$La_6Sc_{0.66}Si_2S_{14}$ [a]	0.6		

[a] The magnetic shielding constants for these materials could not be calculated due to the positional disorder in the crystal structure.

Table S6. Experimental and DFT-calculated ^{45}Sc NMR parameters.

Sample	Experimental				Calculated		
	δ_{iso}(^{45}Sc) / ppm	C_Q / MHz	η	P_Q / MHz	$\lvert C_Q \rvert$ / MHz	η	$\lvert P_Q \rvert$ / MHz
$La_6Sc_{0.67}Si_2S_{14}$	472.2			3.0	2.0(2)	0.17(5)	2.0(2)
$La_6Sc_{0.67}Ge_2S_{14}$	474.5			2.8			
$LaScS_3$	377.2	8.4	0.28	8.5	6.52	0.28	6.60

Table S7. Second harmonic generation (SHG) signal for select compounds.

Particle size (μm)	**38.5-54**	**54-88**	**88-105**	**105-150**	**150-200**
Phase	**SHG Intensity (mV)**				
$AgGaS_2$	15.0	26.0	35.0	80.0	113.0
$La_6CoSi_2S_{14}$	0.8	0.8	0.8	0.8	0.8
$La_6Rh_{0.67}Si_2S_{14}$	14.0	12.8	13.6	-	13.0
$La_6Ir_{0.67}Si_2S_{14}$	13.5	13.6	13.2	12.2	12.6
$La_6Cu_2Si_2S_{14}$	1.5	1.3	0.8	0.75	0.8
$La_6Cu_2Ge_2S_{14}$	20	24	37	-	-
$La_6Ag_2Si_2S_{14}$	0.4	0.4	0.3	-	-
$La_6Au_2Si_2S_{14}$	7.7	6.8	-	1.5	2.4

Table S8A. A summary of structural data for $La_6(TM)_xSi_2S_{14}$. O_h = octahedron

Metal	Ox. State/ Spin state	R_{ion}[a] (Å)	R_{calc}[b]	$V_{Oh\text{-}full}$(Å^3)	$V_{Oh\text{-}empty}$(Å^3)	V_{full}/V_{empty}	$d_{M\text{-}S}$ for filled O_h			*a*/*c*	V (Å^3)
							Min (Å)	Max (Å)	d_{min}/d_{max}		
Sc	3	0.75	0.77	23.53	28.94	0.81	2.605	2.608	0.999	1.798	531.9
Ti	3	0.67	0.73	22.49	29.91	0.75	2.562	2.569	0.997	1.784	529.9
V	2	0.79	0.71	22.12	27.27	0.81	2.551	2.552	1.000	1.795	526.6
	3	0.64									
Cr	3	0.62	0.70	21.87	28.95	0.76	2.537	2.546	0.996	1.789	527.2
Mn	2/hs	**0.83**	0.81	24.77	-	-	2.640	2.660	0.992	1.804	529.9
	2/ls	0.67									
Fe	2/hs	0.61	0.78	23.87	-	-	2.610	2.620	0.996	1.795	527.2
	2/ls	0.78									
Co	2/hs	0.65	0.78	23.91	-	-	2.610	2.630	0.992	1.793	523.5
	2/ls	0.75									
Ni	2	0.69	0.75	23.14	-	-	2.590	2.590	1.000	1.793	523.5
Zr	4	0.72	0.81	24.62	28.53	0.86	2.636	2.659	0.991	1.793	530.6
Rh	3	0.67	0.70	21.83	28.93	0.76	2.538	2.541	0.999	1.783	523.2
Hf	4	0.71	0.72	22.3	27.30	0.82	2.538	2.579	0.984	1.791	531.2
Pt	4	**0.63**	0.76	23.35	30.60	0.76	2.594	2.604	0.996	1.776	525.5

[a] Ionic radii taken from Shannon,[10] min and max observed values are highlighted in bold.

[b] Radii are calculated by subtracting ionic radius of S^{2-} (Shannon[10]) from the average value of *TM*-S bond.

Table S8B. Ionic radii for select transition metals in octahedral environment. Values highlighted in green lie between 0.63 and 0.83 Å, a proposed range to form target quaternary sulfides $La_6(TM)_xSi_2S_{14}$.

Metal	Ox. State	R_{ion}, Å[a]
Pd	2 square planar	0.64
	2 O_h	0.86
Ru	3	0.68
	4	0.62
Ir	3	0.68
Nb	3	0.72
	4	0.68
	5	0.64
Mo	3	0.69
	4	0.65
	5	0.61
	6	0.59
Ta	3	0.72
	4	0.68
	5	0.64
W	4	0.66
	5	0.62
	6	0.60
Re	4	0.63
	5	0.58
	6	0.55
	7	0.53
Os	4	0.63
	5	0.58
	6	0.55
	7	0.53

[a] Ionic radii taken from Shannon[10].

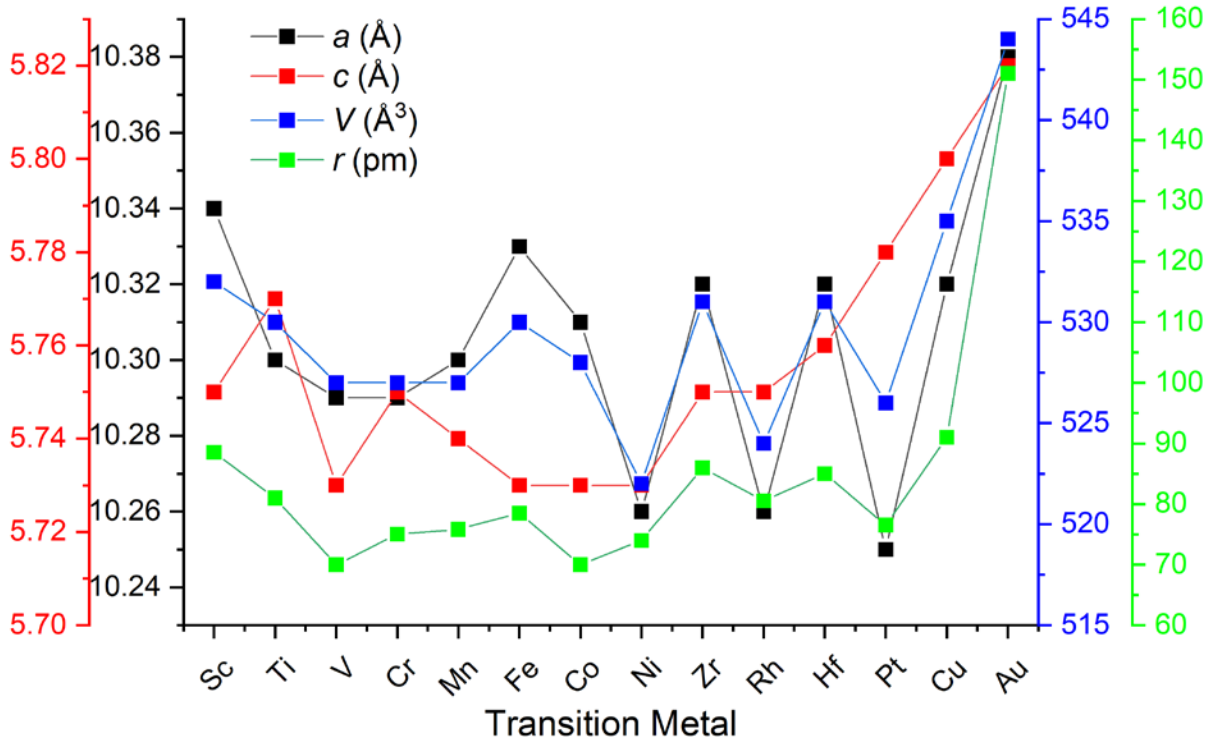

Figure S1. Correlation of hexagonal unit cell parameters (*a* and *c*), unit cell volume and ionic radii[10] for metals for $La_6(TM)_xSi_2S_{14}$ (x = 2 – 0.5).

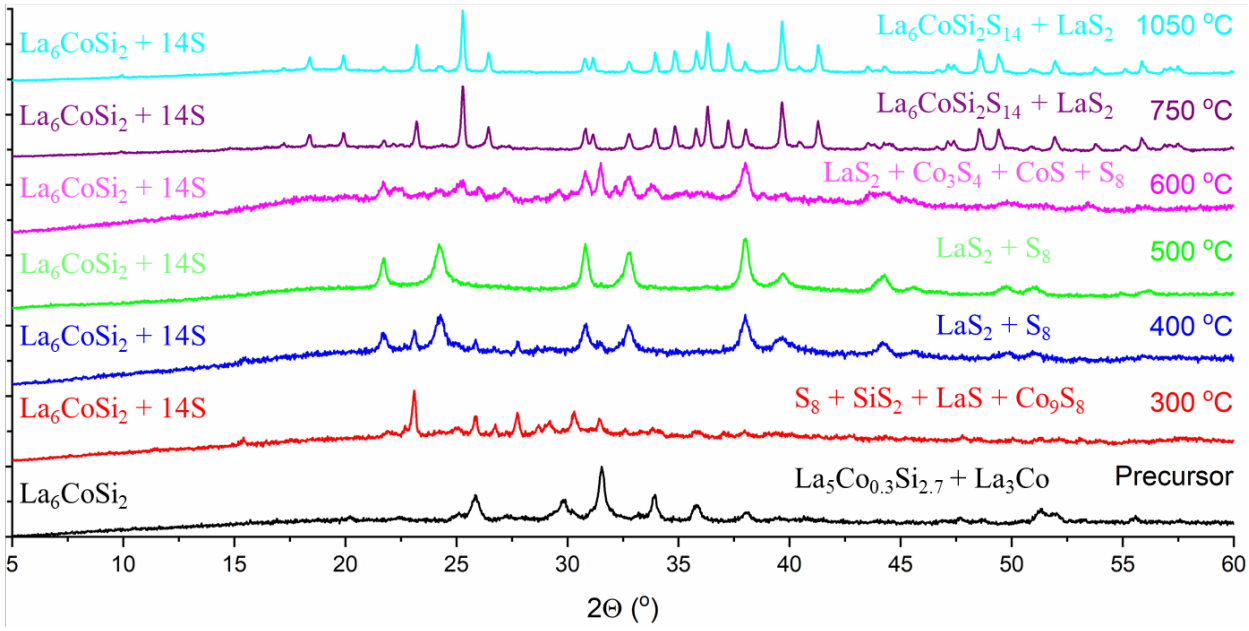

Figure S2. *Ex-situ* PXRD patterns showing phase formation in the $La_6CoSi_2S_{14}$ system. Each pattern represents a different reaction with corresponding maximum reaction temperature. The pre-arc-melted "La_6CoSi_2" and S reactants form $La_6CoSi_2S_{14}$ (*P6*$_3$) at ~750 ºC.

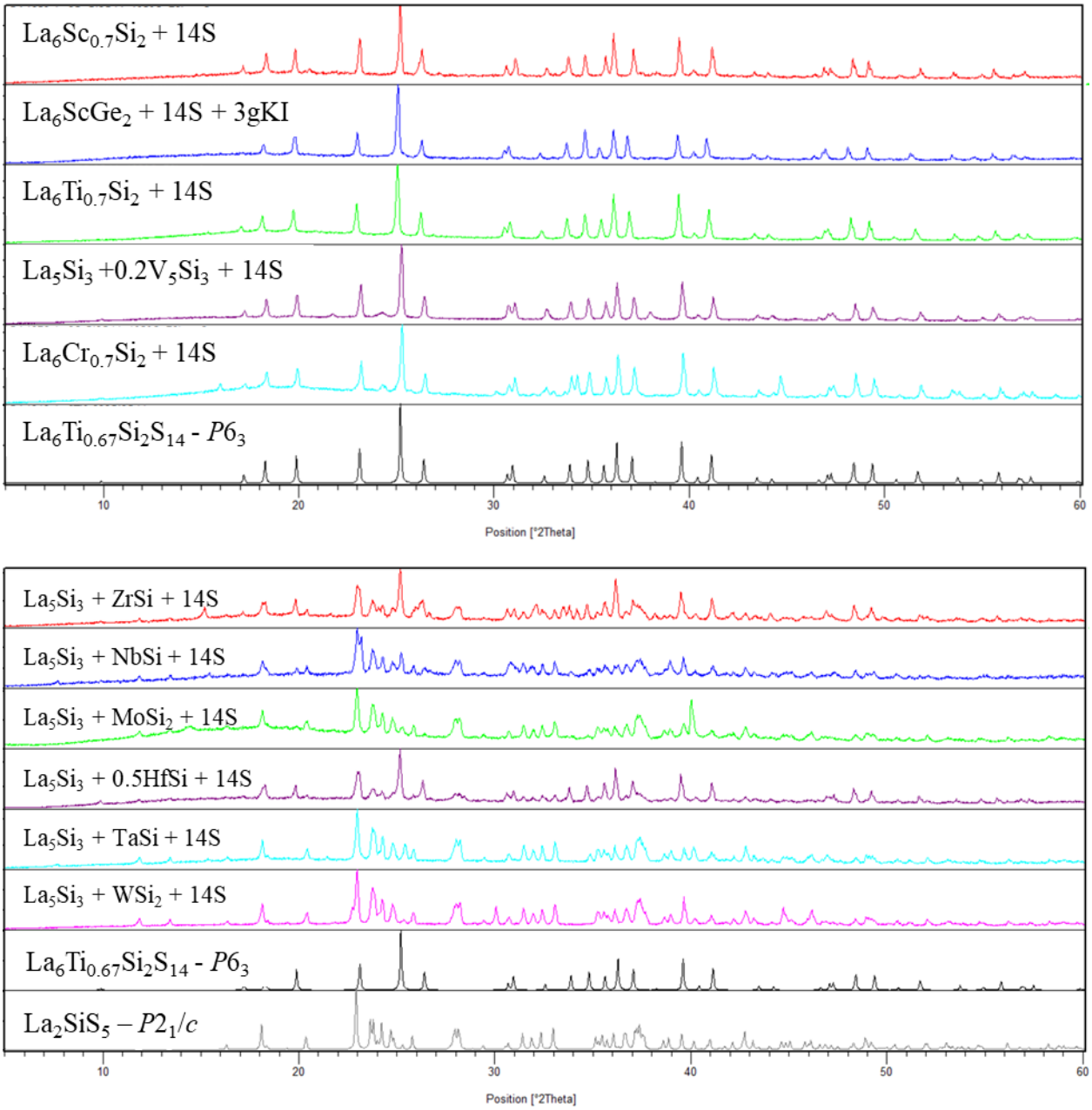

Figure S3A. PXRD patterns for $La_6(TM)_x(Tt)_2S_{14}$ (x = 2 – 0.5) samples: (**top**) *TM* = Sc - Cr, *Tt* = Si and Ge; (**bottom**) *TM* = Zr – W, *Tt* = Si. Patterns in black and grey are for reference. Pattern for La_2SiS_5 is taken from ICSD 240952. Experimental conditions are given in **Table S3A**.

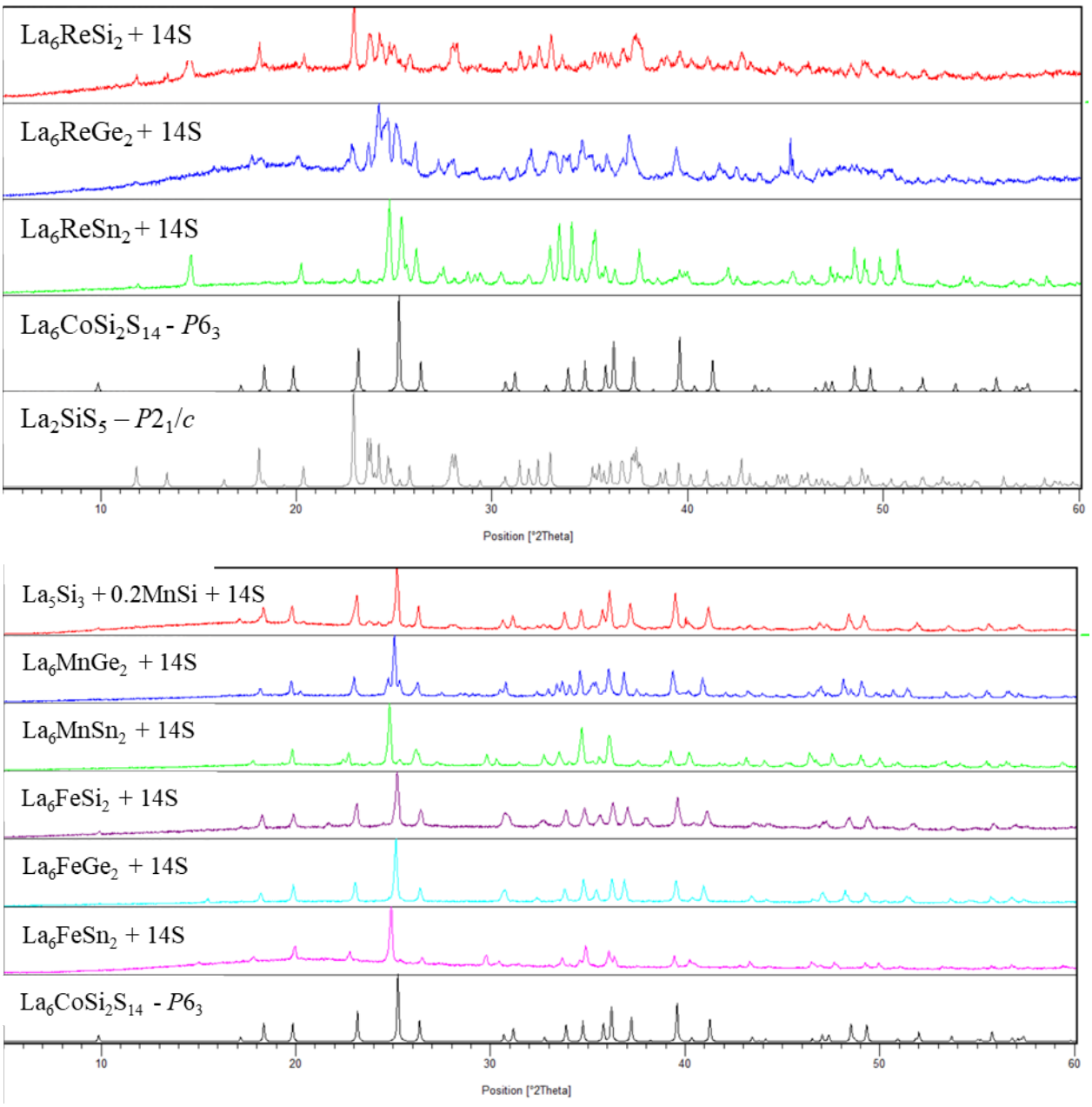

Figure S3B. PXRD patterns for $La_6(TM)_x(Tt)_2S_{14}$ (x = 2 – 0.5) samples: (**top**) *TM* = Re, *Tt* = Si; (**bottom**) *TM* = Mn and Fe, *Tt* = Si, Ge and Sn. Patterns in black and grey are for reference. Pattern for La_2SiS_5 is taken from ICSD 240952. Experimental conditions are given in **Table S3A**.

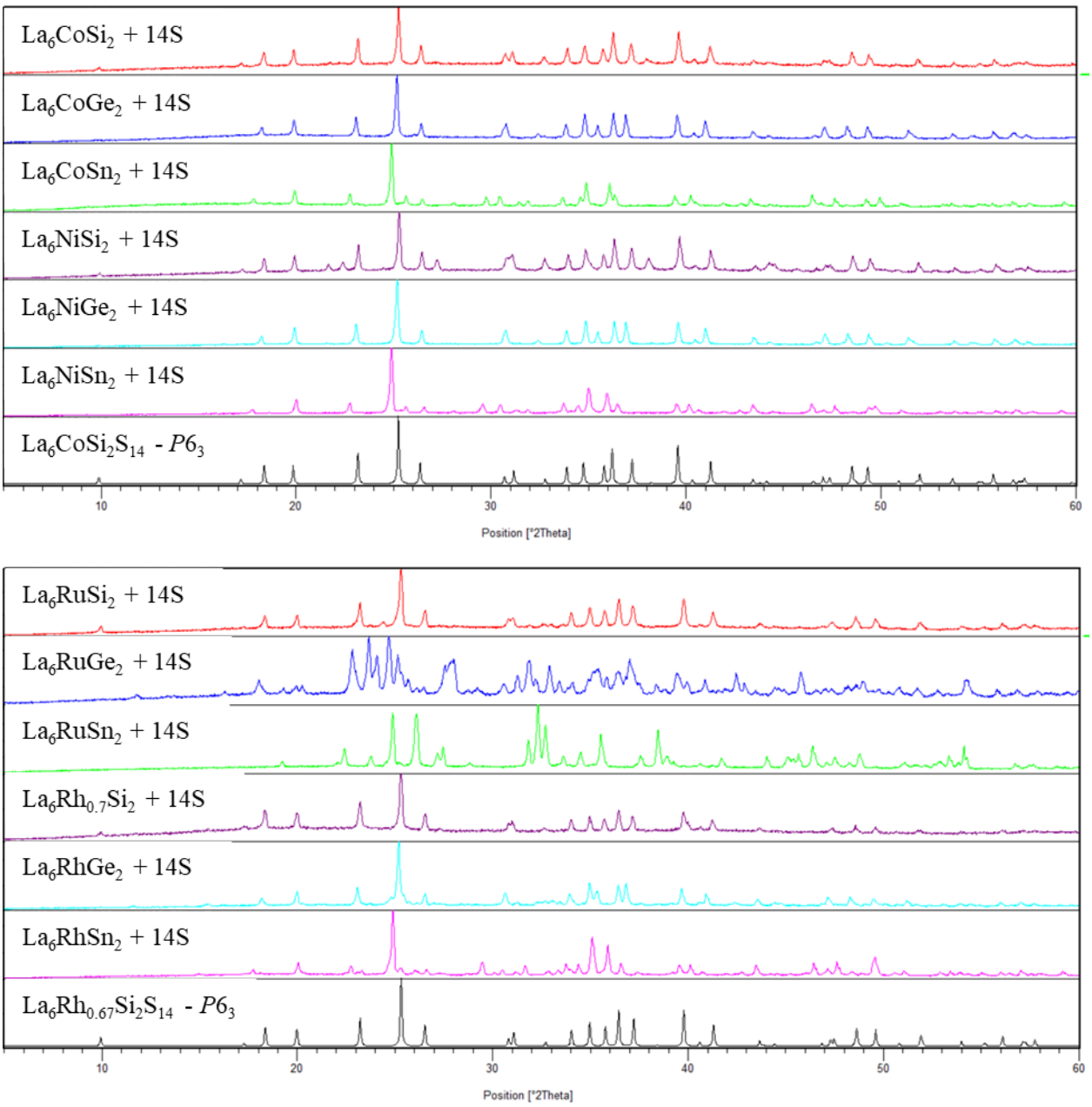

Figure S3C. PXRD patterns for $La_6(TM)_x(Tt)_2S_{14}$ (x = 2 – 0.5) samples: (**top**) *TM* = Co and Ni, *Tt* = Si, Ge, and Sn; (**bottom**) *TM* = Ru and Rh, *Tt* = Si, Ge and Sn. Patterns in black and grey are for reference. Experimental conditions are given in **Table S3A**.

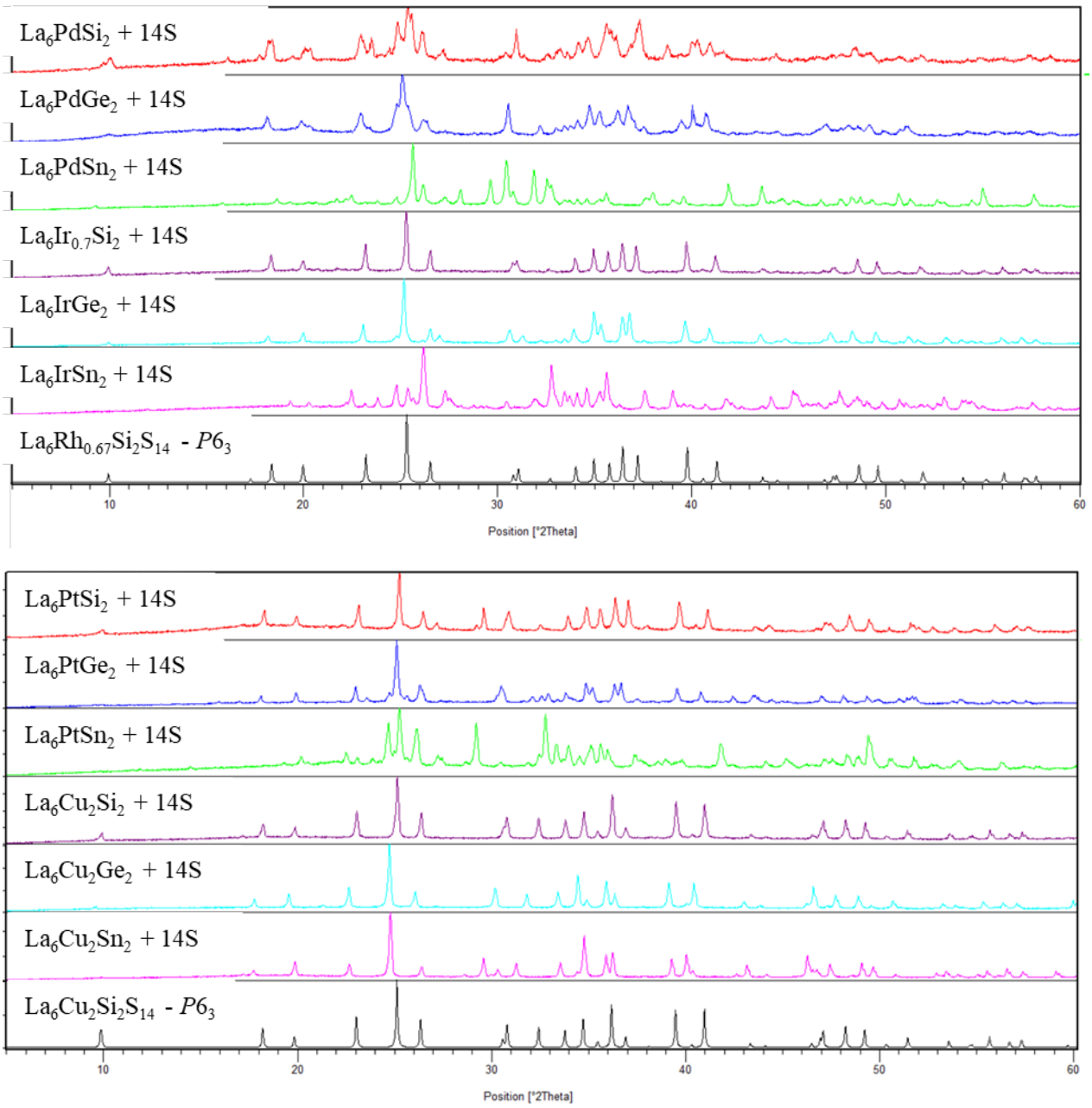

Figure S3D. PXRD patterns for $La_6(TM)_x(Tt)_2S_{14}$ (x = 2 – 0.5) samples: (**top**) *TM* = Pd and Ir, *Tt* = Si, Ge and Sn; (**bottom**) *TM* = Pt and Cu, *Tt* = Si, Ge, and Sn. Patterns in black and grey are for reference. Experimental conditions are given in **Table S3A**.

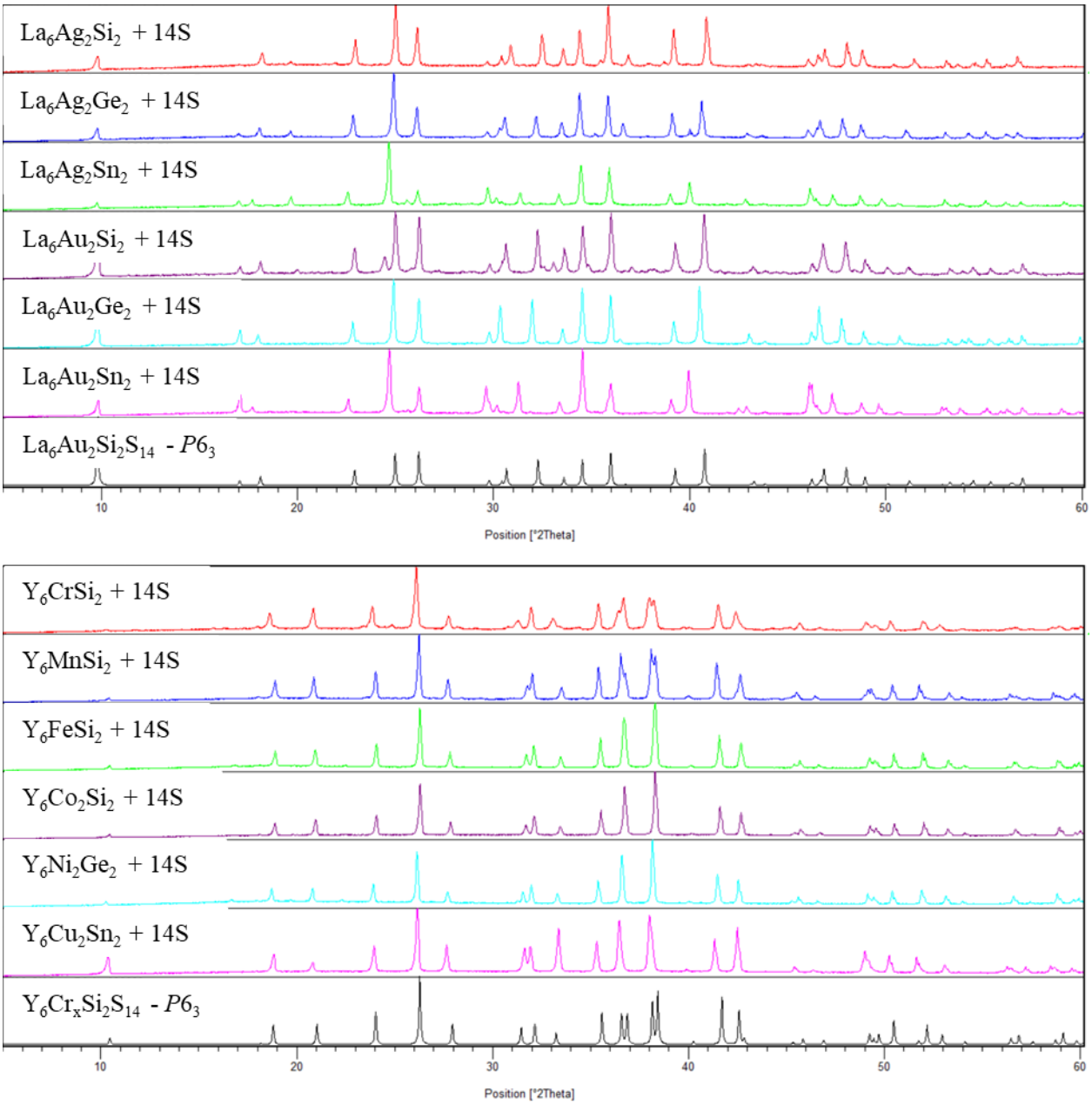

Figure S3E. PXRD patterns for $(RE)_6(TM)_x(Tt)_2S_{14}$ (x = 2 – 0.5) samples: (**top**) *RE* = La, *TM* = Ag and Au, *Tt* = Si, Ge, and Sn; (**bottom**) *RE* = Y, *TM* = Cr - Cu. Patterns in black and grey are for reference. Pattern for $Y_6Cr_xSi_2S_{14}$ is taken from ICSD 626629. Experimental conditions are given in **Table S3A**.

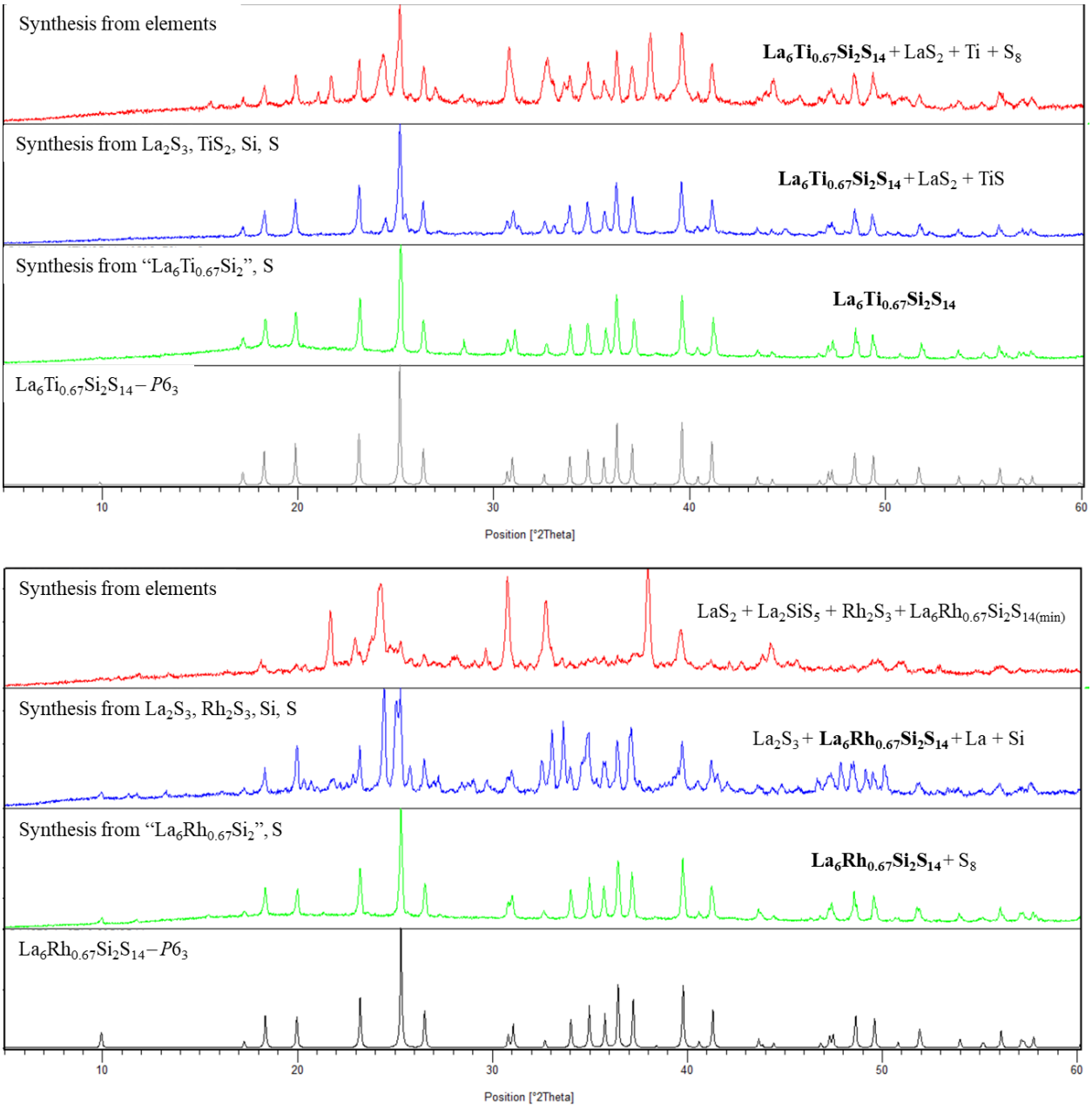

Figure S3F. PXRD patterns for $La_6(TM)_{0.67}Si_2S_{14}$ prepared from elements and binary sulfides and compared to the PXRD pattern for synthesis using a metal silicide precursor. (T**op**) *TM* = Ti; (**bottom**) *TM* = Rh. Patterns in black are calculated from single crystal data. Reaction conditions such as sample scale, ampoule size, ramping and annealing time, and temperature are identical for all shown samples.

TM	Mn			Fe			Co			Ni			Cu		
Color	X														
E_g (eV)	NSP	2.2	2.02	1.67	1.77	1.8	1.85	1.87	1.75	1.95	1.9	1.77	2.6	2.57	2.14
TM	Tc			Ru			Rh			Pd			Ag		
Color					X	X		X		X		X			
E_g (eV)				1.64	NSP	NSP	2.01	NSF	1.88	NSP	1.5	NSP	2.25	1.63	1.76
TM	Re			Os			Ir			Pt			Au		
Color	X	X	X						X			X			
E_g (eV)	No phase	No phase	No phase				2.18	2.14	NSP	1.8	1.69	NSP	2.36	2.54	1.92

Figure S4. Optical images and band gap values (eV) for $La_6(TM)_x(Tt)_2S_{14}$ (*TM* = group 7 - 11; *Tt* = Si, Ge, and Sn; $x = 2 – 0.5$) samples. Only cases where single-phase bulk samples could be acquired were measured. For each metal, the first column is data for Si, second for Ge, and third for Sn. *NSP*= not a single-phase sample; *No phase* = quaternary phase formation was not observed. Extensive temperature optimization was not performed for Sn-containing samples which require lower synthetic temperatures than Si- and Ge-containing analogues.

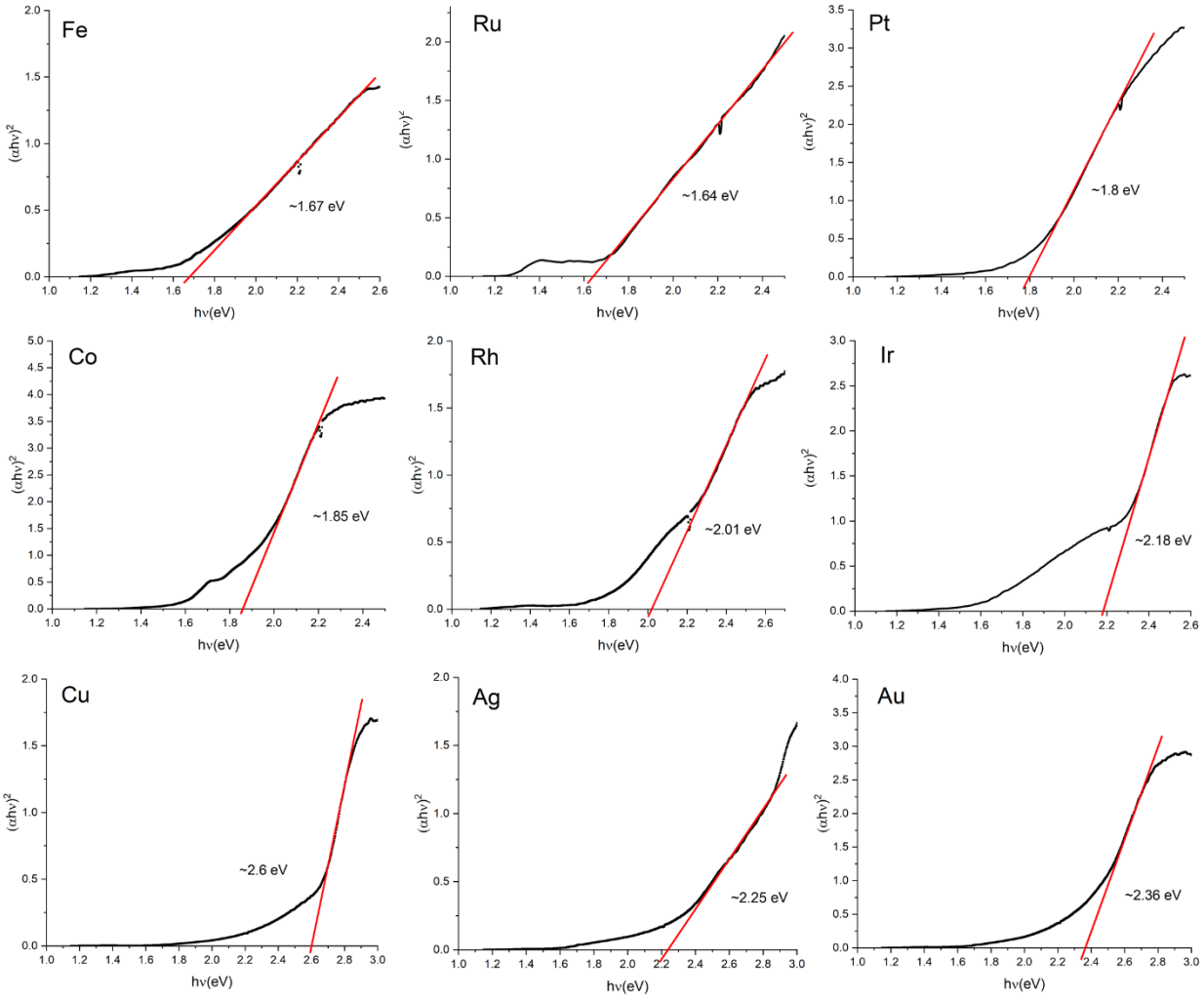

Figure S5. Tauc plots for select compositions for $La_6(TM)_xSi_2S_{14}$ (*TM* = Fe, Co, Ru, Rh, Ir, Pt, Cu, Ag and Au; $x = 2 – 0.5$) plotted as direct band gap materials.

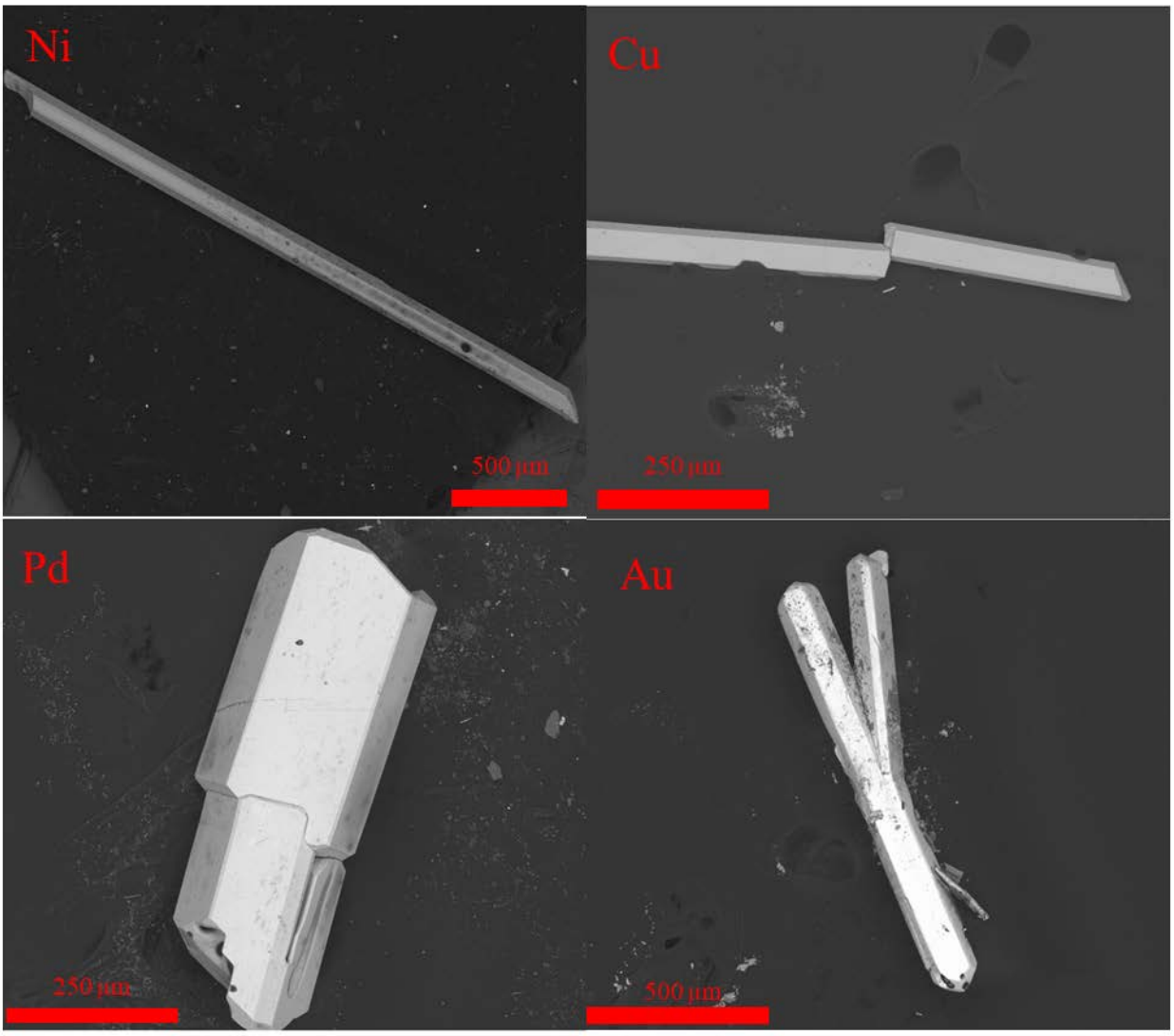

Figure S6. SEM BSE images of select crystals of $La_6(TM)_xSi_2S_{14}$ (*TM* = Ni, Cu, Pd and Au; x = 2 – 0.5). The magnifications are 50x, 150x, 150x and 80x, for Ni, Cu, Pd and Au, respectively.

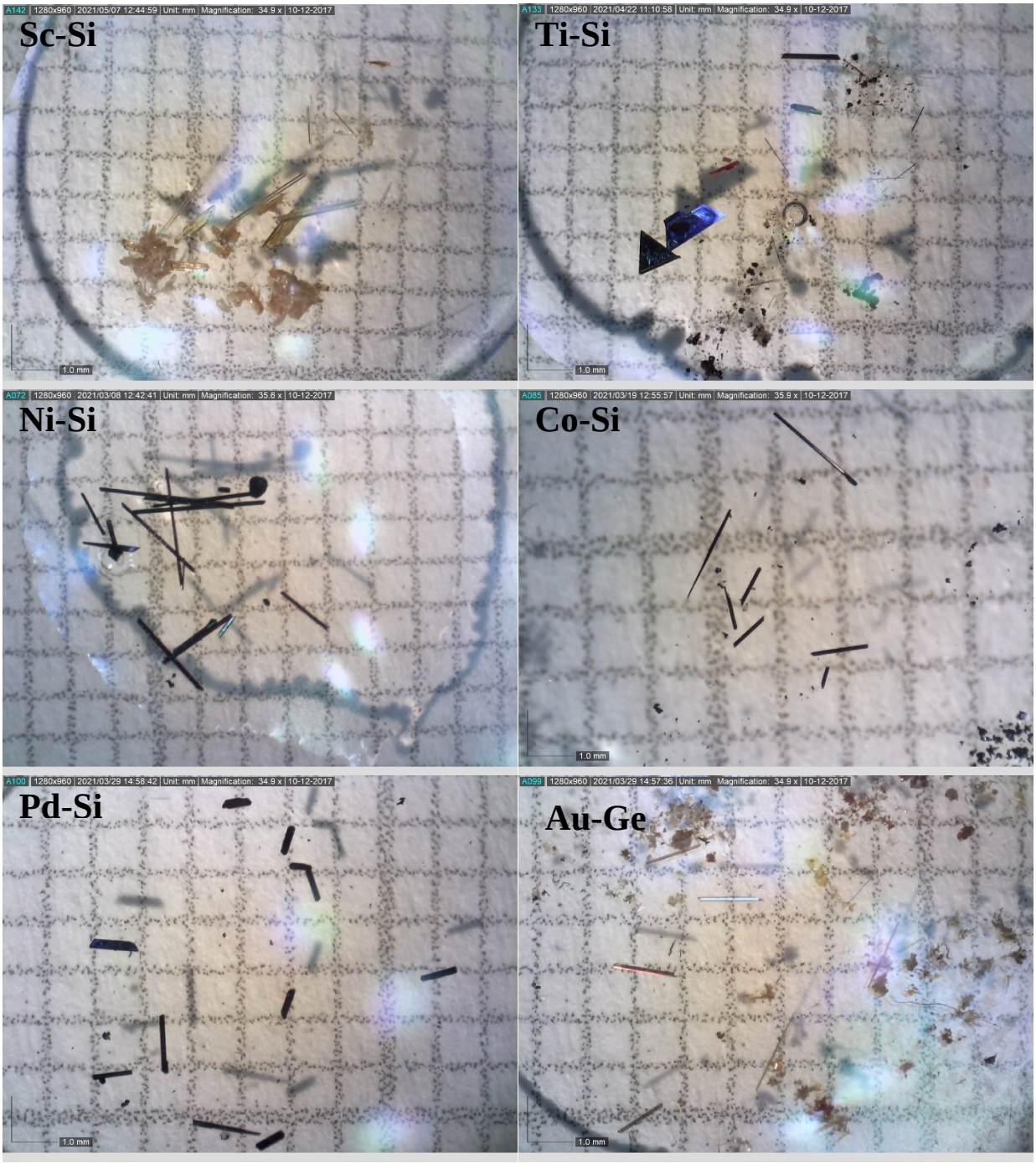

Figure S7. Optical microscope images of select crystals for $La_6(TM)_x(Tt)_2S_{14}$ (*TM* = Sc, Ti, Ni, Co, Pd and Au; *Tt* = Si and Ge; $x = 2 – 0.5$). Each cell on the graph paper is 1×1 mm.

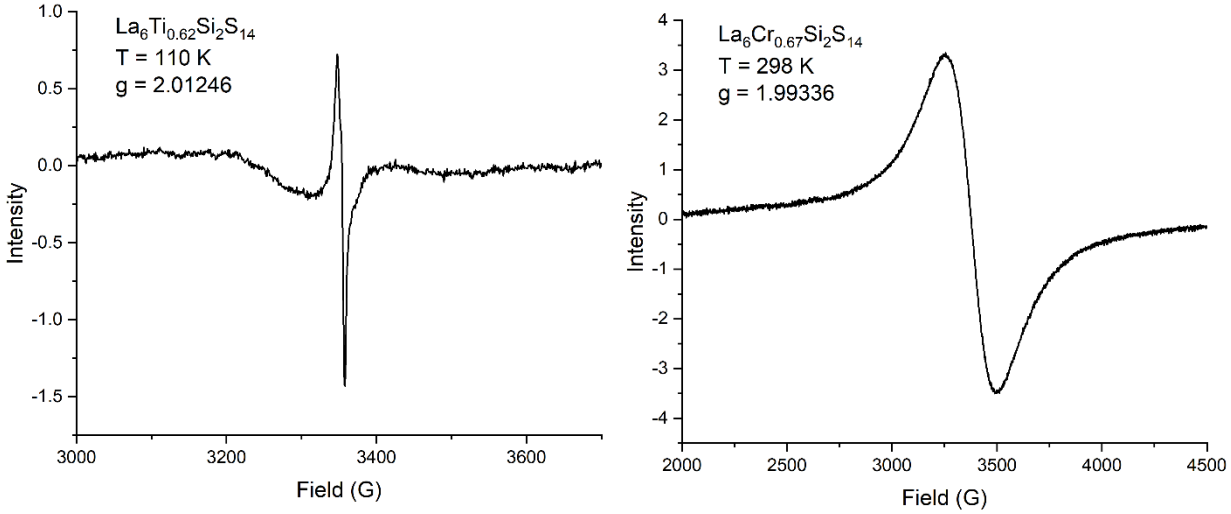

Figure S8. EPR data for $La_6(TM)_{0.67}Si_2S_{14}$ (*TM* = Ti and Cr), showing Ti^{3+} and Cr^{3+} with *g* values of 2.01246 and 1.99336, respectively.[11,12] $La_6V_{0.77}Si_2S_{14}$ sample did not produce a good-intensity signal down to 6 K.

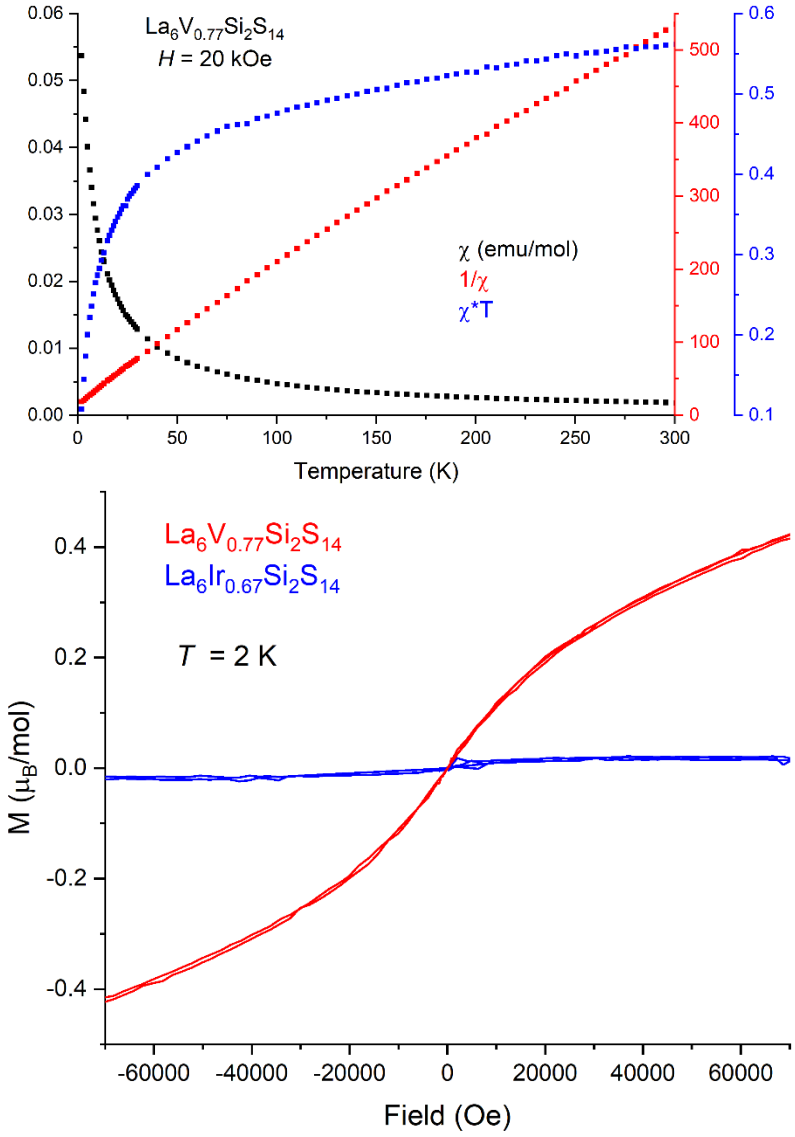

Figure S9. Top: Magnetic data (χ, χ^{-1} and χ*T) for $La_6V_{0.77}Si_2S_{14}$; Bottom: isothermal moment versus field at 2 K for $La_6V_{0.77}Si_2S_{14}$ and $La_6Ir_{0.67}Si_2S_{14}$ (**bottom**).

References

(1) Sheldrick, G. M. A Short History of *SHELX*. *Acta Crystallogr A Found Crystallogr* **2008**, *64* (1), 112–122. https://doi.org/10.1107/S0108767307043930.

(2) Massiot, D.; Fayon, F.; Capron, M.; King, I.; Le Calvé, S.; Alonso, B.; Durand, J.-O.; Bujoli, B.; Gan, Z.; Hoatson, G. Modelling One- and Two-Dimensional Solid-State NMR Spectra: Modelling 1D and 2D Solid-State NMR Spectra. *Magn. Reson. Chem.* **2002**, *40* (1), 70–76. https://doi.org/10.1002/mrc.984.

(3) Massiot, D.; Hiet, J.; Pellerin, N.; Fayon, F.; Deschamps, M.; Steuernagel, S.; Grandinetti, P. J. Two-Dimensional One Pulse MAS of Half-Integer Quadrupolar Nuclei. *Journal of Magnetic Resonance* **2006**, *181* (2), 310–315. https://doi.org/10.1016/j.jmr.2006.05.007.

(4) Clark, S. J.; Segall, M. D.; Pickard, C. J.; Hasnip, P. J.; Probert, M. I. J.; Refson, K.; Payne, M. C. First Principles Methods Using CASTEP. *Zeitschrift für Kristallographie* **2005**, *220*, 567–570.

(5) Pickard, C. J.; Mauri, F. All-Electron Magnetic Response with Pseudopotentials: NMR Chemical Shifts. *Phys. Rev. B* **2001**, *63* (24), 245101. https://doi.org/10.1103/PhysRevB.63.245101.

(6) Yates, J. R.; Pickard, C. J.; Mauri, F. Calculation of NMR Chemical Shifts for Extended Systems Using Ultrasoft Pseudopotentials. *Phys. Rev. B* **2007**, *76* (2), 024401. https://doi.org/10.1103/PhysRevB.76.024401.

(7) Perdew, J. P.; Burke, K.; Ernzerhof, M. Generalized Gradient Approximation Made Simple. *Phys. Rev. Lett.* **1996**, *77* (18), 3865–3868. https://doi.org/10.1103/PhysRevLett.77.3865.

(8) Eckert, H.; Zhang, Z.; Kennedy, J. H. Glass Formation in Non-Oxide Chalcogenide Systems. Structural Elucidation of Li2S-SiS2-LiI Solid Electrolytes by Quantitative 29Si, 6Li and 7Li High Resolution Solid State NMR Methods. *Journal of Non-Crystalline Solids* **1989**, *107*, 271–282.

(9) Evers, J.; Mayer, P.; Möckl, L.; Oehlinger, G.; Köppe, R.; Schnöckel, H. Two High-Pressure Phases of SiS_2 as Missing Links between the Extremes of Only Edge-Sharing and Only Corner-Sharing Tetrahedra. *Inorg. Chem.* **2015**, *54* (4), 1240–1253. https://doi.org/10.1021/ic501825r.

(10) Shannon, R. D. Revised Effective Ionic Radii and Systematic Studies of Interatomic Distances in Halides and Chalcogenides. *Acta Crystallographica Section A Foundations of Crystallography* **1976**, *A32*, 751–767. https://doi.org/10.1107/S0567739476001551.

(11) Galeev, A. A.; Khasanova, N. M.; Rudowicz, C.; Shakurov, G. S.; Bykov, A. B.; Bulka, G. R.; Nizamutdinov, N. M.; Vinokurov, V. M. Multifrequency EPR Study of Cr^{3+} Ions in $LiScGeO_4$. *J. Phys.: Condens. Matter* **2000**, *12* (20), 4465–4473. https://doi.org/10.1088/0953-8984/12/20/302.

(12) Lombard, P.; Ollier, N.; Boizot, B. EPR Study of Ti3+ Ions Formed under Beta Irradiation in Silicate Glasses. *Journal of Non-Crystalline Solids* **2011**, *357* (7), 1685–1689. https://doi.org/10.1016/j.jnoncrysol.2010.12.015.